Cell Reports

Article

CrrB Positively Regulates High-Level Polymyxin Resistance and Virulence in *Klebsiella pneumoniae*

Graphical Abstract

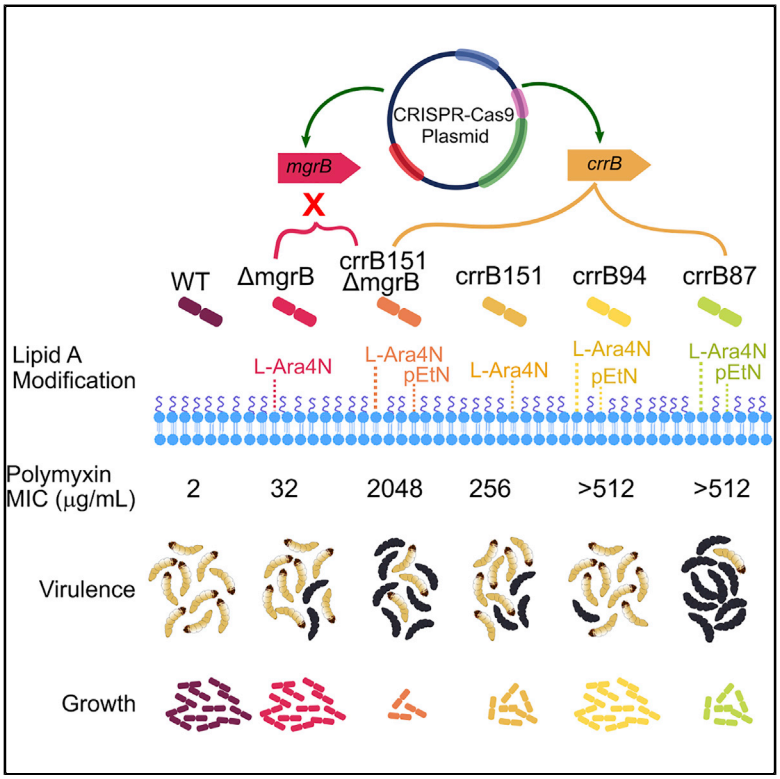

Highlights

- Mutations (SNPs) in *crrB* induce high-level polymyxin resistance and virulence
- *CrrB* SNPs mediate the addition of both L-Ara4N and pEtN to lipid A
- *CrrB* SNPs alter carbon metabolism including the pentose phosphate pathway
- These changes lead to an increase in bacterial virulence at a fitness cost

Authors

Thomas H. McConville,
Medini K. Annavajhala,
Marla J. Giddins, ..., Filippo Mancia,
M. Stephen Trent, Anne-Catrin Uhlemann

Correspondence

au2110@columbia.edu

In Brief

McConville et al. leverage CRISPR-Cas to demonstrate that mutations in *crrB* induce high-level polymyxin resistance in *Klebsiella pneumoniae* via the addition of L-Ara4N and pEtN to lipid A. *CrrB* mutations also increase virulence while conferring a fitness cost and alter carbon metabolism through activation of the pentose phosphate pathway.

McConville et al., 2020, Cell Reports *33*, 108313
October 27, 2020
https://doi.org/10.1016/j.celrep.2020.108313

CellPress

Cell Reports

CellPress
OPEN ACCESS

Article

CrrB Positively Regulates High-Level Polymyxin Resistance and Virulence in *Klebsiella pneumoniae*

Thomas H. McConville,[1] Medini K. Annavajhala,[1] Marla J. Giddins,[1] Nenad Macesic,[1,2] Carmen M. Herrera,[3] Felix D. Rozenberg,[1] Gitanjali L. Bhushan,[4] Danielle Ahn,[4] Filippo Mancia,[5] M. Stephen Trent,[3] and Anne-Catrin Uhlemann[1,6,*]

[1]Division of Infectious Diseases, Department of Medicine, Columbia University Irving Medical Center, New York, NY 10032, USA
[2]Department of Infectious Diseases, The Alfred Hospital and Central Clinical School, Monash University, Melbourne, 3004 VIC, Australia
[3]Departments of Infectious Diseases, College of Veterinary Medicine, University of Georgia, Athens, GA 30602, USA
[4]Division of Pediatric Critical Care, Department of Pediatrics, Columbia University Irving Medical Center, New York, NY 10032, USA
[5]Department of Physiology, Columbia University, New York, NY 10032, USA
[6]Lead Contact
*Correspondence: au2110@columbia.edu
https://doi.org/10.1016/j.celrep.2020.108313

SUMMARY

Polymyxin resistance (PR) threatens the treatment of carbapenem-resistant *Klebsiella pneumoniae* (CRKP) infections. PR frequently arises through chemical modification of the lipid A portion of lipopolysaccharide. Various mutations are implicated in PR, including in three two-component systems—CrrA/B, PmrA/B, and PhoP/Q—and the negative regulator MgrB. Few have been functionally validated. Therefore, here we adapt a CRISPR-Cas9 system to CRKP to elucidate how mutations in clinical CRKP isolates induce PR. We demonstrate that CrrB is a positive regulator of PR, and common clinical mutations lead to the addition of both 4-amino-4-deoxy-L-arabinose (L-Ara4N) and phosphethanolamine (pEtN) to lipid A, inducing notably higher polymyxin minimum inhibitory concentrations than *mgrB* disruption. Additionally, *crrB* mutations cause a significant virulence increase at a fitness cost, partially from activation of the pentose phosphate pathway. Our data demonstrate the importance of CrrB in high-level PR and establish important differences across *crrB* alleles in balancing resistance with fitness and virulence.

INTRODUCTION

Carbapenem-resistant *Enterobacteriaceae* (CRE) infections, particularly carbapenem-resistant *Klebsiella pneumoniae* (CRKP), continue to be an urgent public health threat (van Duin and Doi, 2017). The polymyxins, including polymyxin B and polymyxin E (colistin), are important therapeutics for CRE. However, emerging polymyxin resistance (PR) is a growing concern worldwide that can critically impair our ability to combat CRE infections (Jeannot et al., 2017). This is reflected in exceedingly high all-cause mortality of PR bloodstream infections, reaching greater than 50% in some reports (Rojas et al., 2017).

Polymyxins are cationic peptides targeting negatively charged components of the bacterial outer membrane, notably lipid A. Chemical modification of lipid A is the predominant mechanism to develop PR in Gram-negative bacteria, due to enzymatic action of ArnT and EptA, which add 4-amino-4-deoxy-L-arabinose (L-Ara4N) and phosphethanolamine (pEtN), respectively (Herrera et al., 2017; Jeannot et al., 2017; Petrou et al., 2016). These modifications add positive charge to the bacterial membrane, which repels the polymyxins. Disruptions in *mgrB*, a small trans-membrane protein that acts as a negative regulator, have been the most well-described mechanisms of PR in *K. pneumoniae.* Inactivating mutations in *mgrB* lead to the derepression of the two-component system *phoP/phoQ*, resulting in the activation of the *arnBCADTEF* operon, which encodes for ArnT (Figure 1). However, in a genomic survey of 164 PR clinical isolates, we recently observed that 40% harbored wild-type (WT) *mgrB*. In addition, we identified more than 80 mutations, the majority of which were within three two-component systems—*phoP/Q*, *crrA/B*, and *pmrA/B* (Macesic et al., 2020)—which have been proposed as alternative pathways to PR (Leung et al., 2017; Esposito et al., 2018). In combination with *mgrB*, we will refer to these genes as the "canonical genes." These findings highlight the heterogeneous nature of PR and the urgent need for functional validation of the observed alleles (Macesic et al., 2020).

Thus, while many mutations have been identified as potential or confirmed inducers of PR, the complex genotypic-phenotypic connection, including the corresponding lipopolysaccharide (LPS) modifications, remains incompletely understood. This is in part due to the lack of functional validation of many of the reported mutations due to the absence of tools to efficiently edit genes in multi-drug-resistant (MDR) *K. pneumoniae*. For

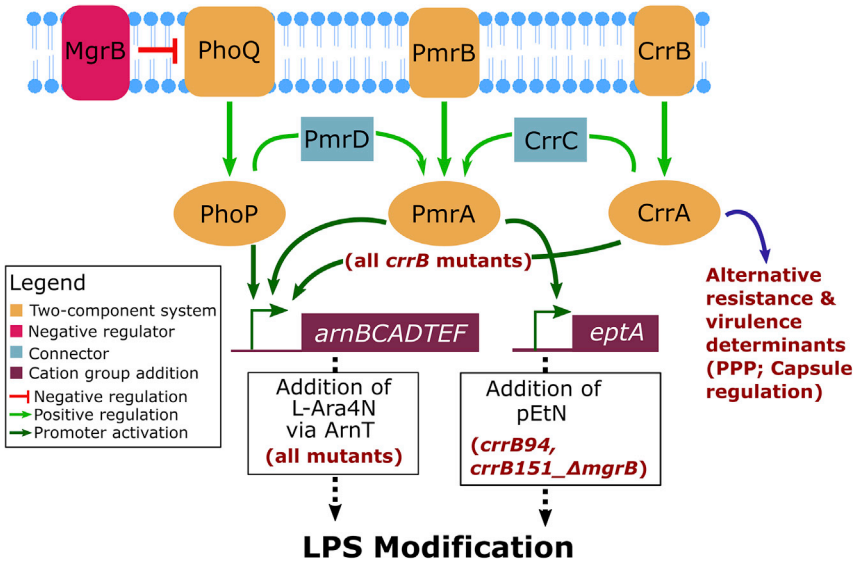

Figure 1. Schematic of the PR Cascade

Proposed schematic of the PR cascade based on previous studies, with noted annotations describing important observations highlighted in this study. PPP, pentose phosphate pathway.

example, mutations in *crrB* have only recently been proposed as an important novel pathway to PR (Cheng et al., 2016, 2018; Jayol et al., 2017). CrrB is a member of the CrrA/B two-component system. Previous work has suggested that this inner membrane bound histidine kinase phosphorylates CrrA, resulting in upregulation of *crrC* and expression of *pmrA/B* (Figure 2). CrrC is a purported connector between the CrrA/B and PmrA/B two-component systems (Cheng et al., 2016). This suggests that *crrB* also induces the *arnBCADTEF* operon (Cheng et al., 2016, 2018; Jayol et al., 2017; Jeannot et al., 2017). Additional studies have taken proteomic and transcriptomic approaches to better understand PR and the role of *crrB* and have supported the observation that CrrA/B activates the *arnBCADTEF* operon (Sun et al., 2020; Ramos et al., 2016). They also suggest that CrrA/B may alter the expression of several carbon metabolism pathways, including gluconeogenesis and the tricarboxylic acid (TCA) cycle. Despite this, conflicting findings exist regarding how CrrB acts on downstream targets, with it being implicated both as a positive and a negative regulator (Cheng et al., 2016, 2018; Jayol et al., 2017)

In light of the importance of the lipid A portion of LPS to activate host immune cells to release pro-inflammatory cytokines including tumor necrosis factor alpha (TNF-α), PR conferring mutations leading to lipid A modifications can significantly impact bacterial pathogenicity and bacterial interactions with the host innate immune system (Ramachandran, 2014). However, there have been conflicting results regarding how PR alters bacterial virulence (Yang et al., 2017; Tietgen et al., 2018; Kidd et al., 2017; Cannatelli et al., 2015). In *K. pneumoniae*, the deletion of *mgrB* leads to increased virulence, while the expression of *mcr-1* in *trans* in *K. pneumoniae* and *E. coli* reduces virulence in the well-described invertebrate model system *Galleria mellonella* (Yang et al., 2017; Tietgen et al., 2018; Nang et al., 2018; Kidd et al., 2017; Cannatelli et al., 2015). This variable virulence phenotype may reflect phenotypic differences between a chromosomal and a plasmid-based mechanism of PR. Alternatively, this may indicate that the addition of L-Ara4N versus pEtN to lipid A, an as-yet-unidentified lipid A modification, or alternative adaptations in resistant isolates mediates differences in the virulence phenotype. Even less is known about the virulence effects of the chromosomal mechanisms of PR in the three two-component systems in *K. pneumoniae.*

To characterize the phenotypic effects of PR in clinical isolates and evaluate if these effects differ in high-level versus low-level resistance, we adapted a CRISPR-Cas9 editing system to CRE. Through single-nucleotide point (SNP) mutation insertions in *crrB* and *arnT* and gene disruptions in *crrA*, *crrB*, *mgrB*, and *pmrA*, we defined the effects of key mutations in these genes on LPS modifications, bacterial fitness, bacterial virulence, and activation of key cellular pathways in CRKP. Taken together, we demonstrate that *crrB* missense variants induce a gain-of-function phenotype that alters multiple cellular processes, leading to not only significantly higher polymyxin minimum inhibitory concentrations (MICs) than *mgrB* disruption, but also changes in bacterial fitness and virulence in CRKP. These findings have important clinical implications on the prevention and management of PR in *K. pneumoniae.* Our easy-to-use CRISPR-Cas9 system provides an important tool to investigate determinants of antimicrobial resistance in drug-resistant CRKP and provides an opportunity to study and inform bacterial-genomics-based predictions of antimicrobial resistance.

RESULTS

Specific *crrB* Mutations Confer a Gain of Function Resulting in High-Level PR

To define the contribution of clinical *crrB* missense mutations to PR in CRKP, we generated isogenic mutants in PR and polymyxin-susceptible (PS) clinical *K. pneumoniae* isolates. We first deleted *crrB* in the PR isolate NR5083 (ST258), harboring *crrB* L87V and *crrA* D26V missense variants, and in NR5452 (ST258), a PS CRKP with a WT copy of *crrB*. The polymyxin B MIC decreased from 64 μg/mL in PR NR5083 to 2 μg/mL in NR5083_*ΔcrrB*, while the MIC for NR5452_*ΔcrrB* remained susceptible at 2 μg/mL. In contrast, deletion of *mgrB* in NR5452 led to an increase in MIC from 2 to 32 μg/mL.

To investigate the contribution of different SNPs in *crrB* on PR, we introduced the three most common *crrB* missense variants seen in our PR *K. pneumoniae* clinical isolates (L87V, L94M, and P151S) into NR5452 (Figure 2) (Macesic et al., 2020). All three mutants (NR5452_*crrB87*, NR5452_*crrB94*, and NR5452_*crrB151*) showed an increase in MIC from 2 μg/mL in

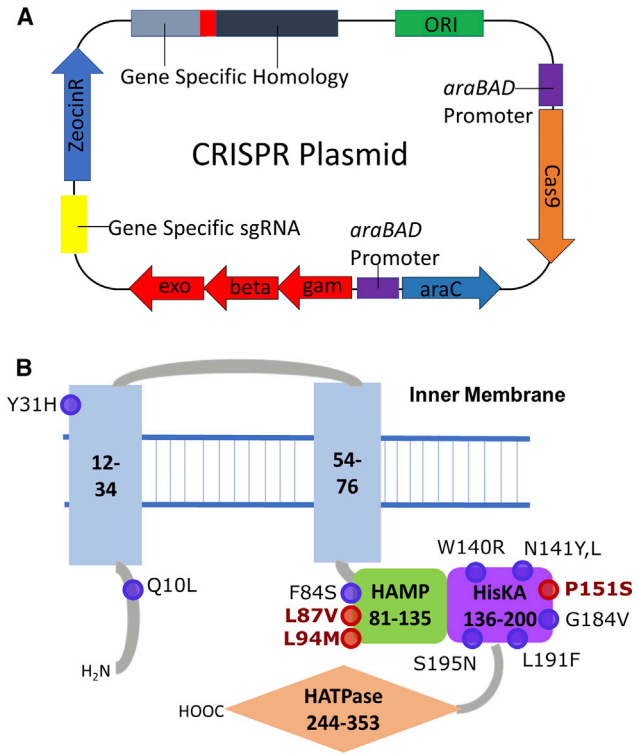

Figure 2. Schematics of the Single-Plasmid CRISPR-Cas9 System and the CrrB Protein

(A) Single-plasmid CRISPR-Cas9 system. Encodes for a *Streptococcus* Cas9 protein, a zeocin resistance gene, the lambda red recombineering genes, and a guide RNA specific to the gene to be modified. The gene-specific homology dictates the type of mutation to be introduced into the genome.

(B) Schematic of the CrrB transmembrane protein. The different domains are shown as labeled shapes. These include two transmembrane domains, a HAMP domain (histidine kinase phosphatase domain), a HisKA domain (histidine kinase A phosphoacceptor domain), and a HATPase domain (histidine kinase ATPase domain). The circles indicate estimated positions of published missense mutations in the CrrB protein; shown in red are the missense variants characterized in this study.

WT NR5452 to 256 μg/mL or greater, which was notably higher than the MIC for NR5452_Δ*mgrB* (Table 1). These high MICs correlate with high MICs of the corresponding clinical isolates harboring the same *crrB* missense mutations (Table S1).

To elucidate how these SNPs affect the downstream targets of CrrB, we generated *crrA* deletion mutants in PR NR5083 (NR5083_Δ*crrA)* and in a generated isogenic mutant, NR5452_*crrB151* (NR5452_*crrB151*_Δ*crrA*). The polymyxin MIC decreased to 2 μg/mL in both isolates (Table 1). This indicates that missense variants in *crrB* confer PR through CrrA. Complementation of *crrA* in both mutants restored PR (Table S1).

Synergistic Effects of the Multiple Mutations in the PR Cascade

In our collection of 164 PR isolates, we noted that more than 20% harbor two or more mutations in the canonical genes, and isolates with multiple mutations show higher MICs than single mutants (Macesic et al., 2020). In particular, the majority of isolates with *crrA/B* mutations contained additional mutations in two or more canonical genes (9/10). Notably, 7 of these 9 isolates also harbored mutations in *mgrB* (four IS elements, two missense variants, and one start codon loss) (Macesic et al., 2020). To elucidate how additional mutations in the canonical genes affect *crrB*-mediated PR, we thus created a *mgrB* knockout (KO) in NR5452_*crrB151*, a combination seen in clinical isolates. Here, the polymyxin MIC increased to 2048 μg/ml, greater than either single mutant (Table 1). This suggests additional mechanisms of resistance contributing to the MIC.

Modulation of CrrB Downstream Targets

Previous literature suggests that *crrB* missense mutations induce PR via the upregulation of *pmrA/B*, which ultimately activates the entire *arnBCADTEF* operon, including *arnT* (Jeannot et al., 2017; Jayol et al., 2017; Cheng et al., 2016, 2018). This work, however, was done in susceptible laboratory strains of *K. pneumoniae*. To test if the downstream targets of CrrA/B differ in a carbapenem-resistant background, we performed qRT-PCR. We quantified expression levels of *phoP/Q* and *pmrA/B/C/K* in all isogenic mutants compared to WT NR5452. NR5452_Δ*mgrB* and NR5452_*crrB151*_Δ*mgrB* had significant upregulation of *phoP/Q* (fold changes 10.6/10.7 and 8.3/6.9, respectively) (Figure 3), while NR5452_*crrB87* showed modest upregulation of *phoP/Q* (1.9/1.8). All isolates except NR5452_*crrB151* demonstrated significant upregulation of *arnT*, highest in NR5452_Δ*mgrB* (26.8) when compared to all other isolates. NR5452_*crrB94*, NR5452_*crrB151*, NR5452_Δ*mgrB*, and NR5452_*crrB151*_Δ*mgrB* lacked significant upregulation of *pmrA/B/C*. Only NR5452_*crrB87* showed modest upregulation of *pmrB* (1.7) without upregulation of *pmrA/C.*

To examine if polymyxin pressure alters the expression of *crrB* and the other canonical genes, we examined gene expression after all isolates were grown in sub-therapeutic concentrations of polymyxin B (0.1 μg/ml). Gene expression for all isogenic mutants was compared to the WT NR5452 grown in sub-therapeutic polymyxin B. NR5452_*crr94*, NR5452_*crrB151*, and NR5452_Δ*mgrB* showed no difference in expression of *pmrA/B/C* even with polymyxin pressure. In the NR5452_*crrB87* mutant, we observed upregulation of *pmrA/C* in addition to *pmrB*. Similarly, in the NR5452_*crrB151*_Δ*mgrB* double mutant, there was significant upregulation of *pmrA/B/C* with polymyxin pressure (Figure 3).

CrrB Induces PR Primarily through Induction of *arnT* via PmrA

PmrA has been suggested as a critical regulator of the *arnBCADTEF* operon. Previous literature suggests that *crrA/B* activate the *pmrA/B* two-component systems via *crrC* (Cheng et al., 2016). However, the observed modest upregulation of *pmrA* expression in the qRT-PCR experiments suggested possible alternative signaling pathways, independent of PmrA, in the downstream cascade of CrrA/B. We therefore disrupted *pmrA* in NR5452_*crrB87*, NR5452_*crrB94*, NR5452_*crrB151*, and the clinical isolate KP0231, which harbors the same L94M amino acid substitution. In the NR5452_*crrB151*_Δ*pmrA* mutant, the MICs decreased from >256 μg/mL to 4 μg/mL. In the NR5452_*crrB87*_Δ*pmrA* and NR5452_*crrB94*_Δ*pmrA* mutants,

Table 1. Genotypic and Phenotypic Characteristics of PR Isogenic Mutants

Isolate	*crrA* Genotype	*crrB* Genotype	*mgrB* Genotype	*pmrA* Genotype	*arnT* Genotype	Polymyxin B MIC (BMD) (μg/mL)
NR5083	Asp 26 Val	Leu 87 Val	WT	WT	WT	64
NR5083Δ*crrA*	160 bp KO	Leu 87 Val	WT	WT	WT	2
NR5083Δ*crrB*	Asp 26 Val	150 bp KO	WT	WT	WT	2
NR5452	WT	WT	WT	WT	WT	1–2
NR5452Δ*crrA*	150 bp KO	WT	WT	WT	WT	2
NR5452Δ*crrB*	WT	150 bp KO	WT	WT	WT	2
NR5452Δ*pmrA*	WT	WT	WT	150 bp KO	WT	2
NR5452_*crrB87*	WT	Leu 87 Val	WT	WT	WT	>512
NR5452_*crrB87_arnT31*	WT	Leu 87 Val	WT	WT	Asp 31 Ala	4
NR5452_*crrB87_ΔpmrA*	WT	Leu 87 Val	WT	150 bp KO	WT	4–8
NR5452_*crrB94*	WT	Leu 94 Met	WT	WT	WT	>512
NR5452_*crrB94_arnT31*	WT	Leu 94 Met	WT	WT	Asp 31 Ala	4
NR5452_*crrB94_ΔpmrA*	WT	Leu 94 Met	WT	WT	WT	4–8
NR5452_*crrB151*	WT	Pro 151 Ser	full KO	WT	WT	256
NR5452_*crrB151_arnT31*	WT	Pro 151 Ser	full KO	WT	Asp 31 Ala	2
NR5452_*crrB151_ΔcrrA*	150 bp KO	Pro 151 Ser	WT	WT	WT	2
NR5452_*crrB151_ΔpmrA*	WT	Pro 151 Ser	WT	150 bp KO	WT	4
NR5452_*crrB151_ΔmgrB*	WT	Pro 151 Ser	full KO	WT	WT	2048
NR5452Δ*mgrB*	WT	WT	full KO	WT	WT	32
KP0231	WT	Leu 94 Met	WT	WT	WT	>512
KP0231_*ΔpmrA*	WT	Leu 94 Met	WT	150 bp KO	WT	8
KP0231_*arnT31*	WT	Leu 94 Met	WT	WT	Asp 31 Ala	4
NR4448	WT	WT	stop	WT	WT	16
NR4448_*arnT31*	WT	WT	stop	WT	Asp 31 Ala	2

the MIC decreased from >512 μg/mL to between 4 and 8 μg/mL, and in the KP0231_*ΔpmrA*, the MIC decreased from >512 μg/mL to 8 μg/mL. In population analysis, there was a shift toward heteroresistance, defined as subpopulations of an isolate showing significantly more resistance than the main population, in both the KP0231_*ΔpmrA* and the NR5452_*crrB94_ΔpmrA* mutants (Figure 4) (Andersson et al., 2019). Both mutants had subpopulations that grew on concentrations of polymyxin B as high as 32 μg/mL. While these results support that the *pmrA/B* two-component system is activated downstream of CrrB and contributes to PR, they also raise the possibility that a PmrA-independent pathway contributes to PR in these isolates.

To test if ArnT, the final enzyme in *arnBCADTEF* operon that catalyzes the addition of L-Ara4N to lipid A, mediates PR in *crrB* mutants, we edited *arnT* in the isogenic *crrB* mutants. We inserted a D31A amino-acid substitution, which is an enzyme-inactivating mutation that lies within the active site of ArnT (Petrou et al., 2016). In NR5452_*crrB151_arnT31*, the MIC decreased from 256 μg/mL to 2 μg/mL. Likewise, in control isolate NR4448, a PR *K. pneumoniae* clinical isolate with a stop-codon mutation in *mgrB*, the introduction of the D31A mutation decreased the MIC from 16 μg/mL to 2 μg/mL. However, in NR5452_*crrB87*, NR5452_*crrB94*, and KP0231, the D31A mutation decreased polymyxin MICs from >512 μg/mL to 4 μg/mL, which is still within the resistant range. Taken together, ArnT represents a vitally important final step in CrrB-mediated PR. However, our results suggest that in certain *crrB* missense mutants, including L87V and L94M, ArnT-independent mechanisms such as the addition of pEtN contribute to the persistent low-level PR. These mechanisms may account for the notably higher MICs seen in *crrB* missense mutants.

LPS Modification in *crrB* Isogenic Mutants

To directly examine the effect of *crrB* mutations on lipid A, we performed thin layer chromatography (TLC) on all isogenic mutants and the WT NR5452. All *crrB* SNP mutants and the *ΔmgrB* mutant demonstrated doubly modified lipid A (Figure S1). In the *crrB* double mutants where *crrA* or *arnT* were inactivated, these modifications were no longer seen. In contrast, the *crrB* double mutants with *pmrA* inactivation still demonstrated evidence of doubly modified lipid A, again suggesting that *crrB* mutants can activate the *arnBCADTEF* operon independent of *pmrA/B*.

To more definitively identify the lipid A modifications in select isogenic mutants, we carried out matrix-assisted laser desorption/ionization time-of-flight mass spectrometry (MALDI-TOF). First, NR5452_*crrB87* showed the addition of L-Ara4N and pEtN. The *crrB94_ΔpmrA* mutant also showed the addition of L-Ara4N but lacked pEtN. On the other hand, the *crrB94_arnT31* mutant revealed pEtN addition, but not L-Ara4N. The *crrB151* and *ΔmgrB* single mutants had L-Ara4N addition, while similar to *crrB87*, the *crrB151_ΔmgrB* double mutant had the

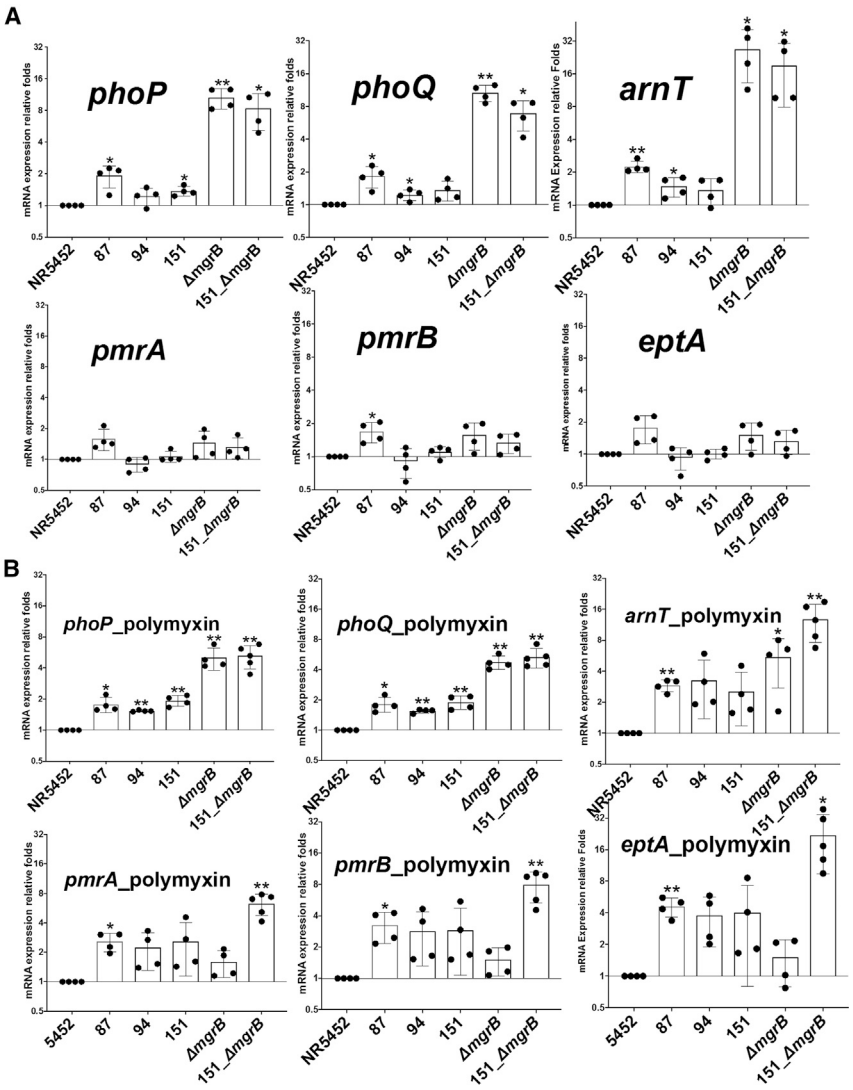

Figure 3. qRT-PCR of Canonical Gene Targets in *crrB* Missense Mutations

Each isolate and target is run in triplicate at least four times. Depicted are gene expression fold changes calculated via the delta/delta ct method. Error bars represent SD between qPCR runs. Significance calculated via t test; *$p < 0.05$, **$p < 0.01$.

(A) Gene expression of the isogenic mutants with RNA extracted after growth in standard Luria-Bertani (LB) Broth.

(B) Gene expression of isogenic mutants with RNA extracted after growth in sub-therapeutic concentrations of polymyxin B.

addition of both L-Ara4N and pEtN (Figure 5). These observations confirm the TLC results where there was consistent evidence of doubly modified lipid A in the PR isogenic mutants. This observation was dependent on an intact *crrA* and *arnT* and in part *pmrA*. Interestingly, the MALDI-TOF results highlight the addition of pEtN in the isogenic mutants with the highest polymyxin MICs.

The *crrB* Isogenic Mutants Show Increased *In Vivo* Virulence Despite Decreased *In Vivo* Growth Rates

To determine if CrrB-mediated mechanisms of PR in *K. pneumoniae* affect bacterial growth, we performed growth kinetics experiments on the isogenic *crrB* mutants. We found that the *crrB87*, *crrB151*, and *crrB151_ΔmgrB* mutants displayed significantly altered growth kinetics in Cation-Adjusted Mueller-Hinton Broth (CAMHB), with shifts of the growth curves to the right compared to the WT, indicating slower growth rates (Figure 6). These results were confirmed for NR5452 and the *crrB151_ΔmgrB* mutant with a standard growth curve in CAMHB measuring colony-forming units (CFUs) over time (data not shown). In contrast, deletion of *mgrB* did not alter the growth kinetics of NR5452 in CAMHB. When grown in increasing concentrations of polymyxin (up to 64 μg/mL), the effect on growth shifted, where *crrB151_ΔmgrB* showed faster growth rates than the WT, and the *crrB151* and *ΔmgrB* mutants at 32 and 64 μg/mL of polymyxin (Figure S2).

Previous studies have yielded conflicting results regarding how PR affects bacterial virulence, where plasmid-encoded *mcr-1* decreases virulence and deletion of *mgrB* increases virulence (Yang et al., 2017; Tietgen et al., 2018; Nang et al., 2018; Kidd et al., 2017; Cannatelli et al., 2015). To determine how *crrB* mutations affect bacterial virulence in *K. pneumoniae*, we compared their virulence in the *G. mellonella* larvae model (Insua et al., 2013; Kidd et al., 2017). We found that WT NR5452 showed minimal killing *of G. mellonella* larvae (1 of 60) over a 72-h period. There was a stepwise increase in larval mortality with *crrB94*, *ΔmgrB*, *crrB151*, *crrB151_ΔmgrB*, and *crrB87* over 72 h. Notably, all isogenic mutants led to significantly higher larval mortality compared to NR5452. *CrrB87* and *crrB151_ΔmgrB* increased mortality to a significantly greater extent than all other mutants ($p < 0.0001$; Figure 6). The observed larval mortality did not correlate with polymyxin B MIC or lipid A modifications. Isolates with slower growth rates tended to induce more larval mortality, but there was not a direct correlation between growth rate and observed virulence.

RNA-Seq Reveals Notable Differences in the Activation of the Downstream Targets of CrrB

To better understand the noted phenotypic variabilities in polymyxin MICs, growth kinetics, and the *G. mellonella* killing assay between *crrB* and *mgrB* mutants, we performed RNA sequencing (RNA-seq). These results reflect the overall transcriptome, as opposed to qRT-PCR, which measures absolute gene expression of specific targets compared to the WT isolate.

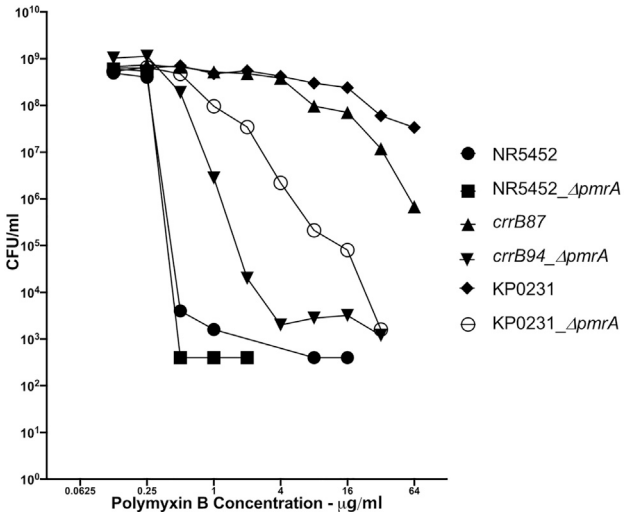

Figure 4. Modified Population Analysis Profiles of a Selection of PR and PS Isogenic Mutants

WT NR5452 is compared to isogenic mutants NR5452_*ΔpmrA*, *crrB87*, *crrB94_ΔpmrA*, KP0231, and KP0231_*ΔpmrA*.

We found that the *ΔmgrB* mutant and the *crrB* SNP mutants showed significantly different transcriptomic profiles (Figure S3). Compared to the WT, there was significant upregulation of *phoP/phoQ* and the *arnBCADTEF* operon in the Δ*mgrB* mutant, consistent with prior literature (Granata and Petrosillo, 2017; Jayol et al., 2015; Jeannot et al., 2017). We also observed significant upregulation of a magnesium transporter and an associated ATPase as well as downregulation of a magnesium/cobalt efflux pump (*corC)*. In contrast, none of these transcripts were upregulated in the *crrB* mutants. In the *crrB151* mutant, we found significant upregulation of transcripts important for glycerolipid/phospholipid metabolism, including the a/b/c subunits of the glycerol-3-phosphate dehydrogenase enzyme (GPDH), when compared to the WT (Figure S3).

In the *crrB151_ΔmgrB* double mutant, there were more than 400 transcripts with significantly altered expression compared to the WT NR5452 that were not up- or downregulated in the *crrB151* and *ΔmgrB* single mutants (Table S2). Notable unique transcripts in the *crrB151_ΔmgrB* mutant included upregulation of several members of the pentose phosphate pathway (PPP). This included the transketolase B enzyme subunit, necessary for the production of distinct carbon intermediates utilized in amino acid and fatty acid metabolism and LPS biosynthesis. There was also altered expression in transcripts involved in capsular biosynthesis, including *barA* and *rcsA.* Finally, we saw increased expression of *pmrA*, which was not seen in either of the single mutants.

To determine if the increase in expression of PPP enzymes in the double mutant influenced the metabolic phenotype of the organism, we measured the extracellular acidification rate (ECAR via Seahorse XFe24 Analyzer - Agilent) in response to glucose and oligomycin as a measure of glycolysis and glycolytic capacity (Figure S4). We found that glycolytic activity was reduced, suggesting shunting of glucose-6-phosphate away from glycolysis and into the PPP. To functionally validate the phenotypes of the *crrB151_ΔmgrB* mutant, we created a triple mutant via KO of the B subunit of the transketolase enzyme creating *crrB151_ΔmgrB_ΔtktB*. Following KO of *tktB*, we observed restoration of glycolysis to that of the parent strain, NR5452. Additionally, the triple mutant was significantly less virulent in the *G. mellonella* model when compared with *crrB151_ΔmgrB* ($p = 0.003$), whereas the polymyxin MIC remained elevated at 2048 μg/mL.

DISCUSSION

Recent advances in microbial genomics have enabled full recognition of an unprecedented diversity of mutations and alterations leading to PR in clinical CRE isolates. However, difficulties in highly efficient gene editing in MDR CRE isolates has precluded systematic analyses of how these diverse genetic backgrounds impact polymyxin MICs and growth and virulence of isolates. Through adaptation of a single-vector CRISPR-Cas9 gene editing system, combined with lambda red recombineering and zeocin as a selectable marker, we were able to demonstrate important functional differences with clinical implications between different PR mutants. We demonstrated that the tested L87V, L94M, and P151S *crrB* mutations are of particular clinical concern because they induce high-level PR and increased virulence in ST258 CRKP through the activation of unique cellular pathways. In contrast, disruption of *mgrB* led to lower MICs and a more modest increase in virulence, while not conferring impaired growth kinetics *in vitro*, as was observed for the *crrB* single mutants and the *crrB151_ΔmgrB* double mutant.

Our results clearly demonstrate that *crrB* missense mutations lead to a gain of function in CRKP. Of further concern is our observation that mutations in multiple components of the cascade, specifically *crrB* and *mgrB*, act synergistically to activate unique cellular pathways that further increase both polymyxin MIC and virulence. These results have far-reaching clinical implications that can inform genomics-based diagnostic and treatment approaches for CRE and PR *K. pneumoniae* infections.

Interestingly, while all three isogenic *crrB* mutants demonstrated an association with high-polymyxin MICs, we noted significant differences in the activation of downstream cascade components, reflected in different lipid A modifications, gene expression profiles, and virulence phenotypes. These differential phenotypes may be explained by the location of SNPs in different domains in the CrrB protein. Amino acids 87 and 94 fall within a histidine kinase phosphatase domain, while amino acid 151 falls within a phospho-acceptor domain of the histidine kinase (Figure 2). Activation of the phosphatase domain versus the phosphor-acceptor domain could lead to differential activation of the CrrA response regulator and the subsequent downstream targets. This was evident after *pmrA* KO in the three *crrB* SNP mutants. In all *crrB_ΔpmrA* mutants, there was only partial restoration of polymyxin B MIC, but MIC was highest, up to 8 μg /ml, in the L87V- and L94M-containing mutants (*crrB87*, *crrB94*, and KP0231). Similarly, through lipid A analysis, we saw addition of L-Ara4N in all *crrB* mutants, which remained after KO of *pmrA*. Editing the catalytic domain of ArnT in the *crrB*

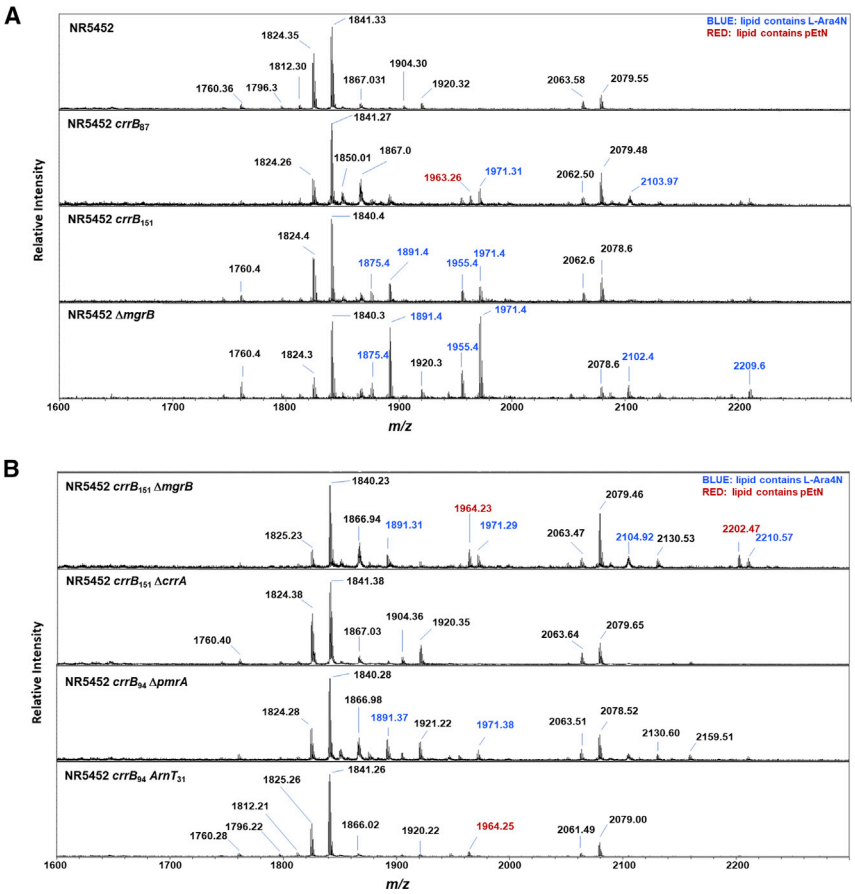

Figure 5. Lipid A Analysis of Isogenic Mutants

(A) Mass spectroscopy of the WT NR5452 and the *crrB87*, *crrB151*, and *ΔmgrB* mutants.

(B) Mass spectroscopy analysis of a selection of double mutants including *crrB151_ΔmgrB*, *crrB151_ΔcrrA*, *crrB94_ΔpmrA*, and *crrB94_ArnT31* mutants. Peaks correspond to specific lipid A modifying groups. Peaks labeled with blue correspond to L-Ara4N, and red corresponds to L-pEtN.

mutants removed L-Ara4N, but it did not completely restore susceptibility in the *crrB87_arnT31*, *crrB94_arnT31*, and KP0231_*arnT31* mutants, where MICs remained in the resistant range. This is likely related to the addition of pEtN, catalyzed via EptA, which was seen on MALDI-TOF analysis of the *crrB87* and *crrB151_ΔmgrB* mutants. This final observation was further supported by qRT-PCR data where the upregulation *eptA* (*pmrC*) was seen in the *crrB87 and crrB151_ΔmgrB* mutants when exposed to sub-therapeutic concentrations of polymyxin B. Taken together, this highlights three observations about the PR cascade in CRKP: (1) the expression of the *arnBCADTEF* operon in *crrB* mutants can be activated independently of *pmrA*/B, (2) there are *arnT*-independent mechanisms of PR in *crrB* missense mutants, and (3) the position of the *crrB* mutations has important implications on the resulting phenotype. This suggests that the CrrA/B two-component system has multiple downstream targets, and certain missense variants may not only increase activation of the response regulator, but may also broaden the set of activated downstream cellular processes.

The concept that the expanded activation of downstream targets of the two-component systems can lead to more significant changes in polymyxin MIC was further validated by the phenotype of the *crrB151_ΔmgrB* mutant. In transcriptomic analysis, the *crrB151_ΔmgrB* mutant showed activation of multiple unique cellular processes that were not activated in the WT NR5452 or either single mutant. We observed significant upregulation of *pmrA*, which was consistent with the qRT-PCR data, where *pmrA/B/C* were upregulated in *crrB151_ΔmgrB* in the presence of polymyxin B. This was supported by lipid A analysis where the *crrB151_ΔmgrB* mutant showed addition of both L-Ara4N (*arnT*) and pEtN (*eptA*), a combination also seen in the *crrB87* mutant. The combination of pEtN and L-Ara4N could increase membrane charge to a greater extent than either modification alone, contributing to the observed rise in MIC. With the increasing use of mass spectroscopy in clinical laboratories, further validation of unique lipid A signatures associated with high-level PR could aid in the development of rapid diagnostic techniques. In addition to lipid A modifications, transcripts involved in regulation of the bacterial capsule, including *barA* and *rcsA*, were differentially expressed in the *crrB151_ΔmgrB* mutant (Dorman et al., 2018). Alteration and release of capsular components could limit polymyxin activity by decreasing access to the outer membrane, which could further increase MIC (2048 μg/mL).

The differential activation of downstream targets may also explain both the decreased growth rates of the *crrB* mutants and the increased *in vivo* virulence as measured in the *G. mellonella* killing assays. Here, while the *crrB87*, *crrB151*, and *crrB151_ΔmgrB* mutants showed the highest virulence of all tested isolates, they also had slower growth kinetics. Interestingly, these observed phenotypic changes between the isogenic mutants did not correlate with polymyxin B MIC or lipid A modifications. All *crrB* SNP mutants (*crrB87*, *crrB94*, *crrB151*, and *crrB151_ΔmgrB*) had a polymyxin B MIC of 256 μg/mL or greater and similar lipid A modifications seen via TLC, but notably different growth kinetics and virulence profiles. The activation of unique cellular processes could explain this phenomenon if the expression of specific pathways led to increased virulence but also a fitness cost. The transcriptomic analysis of the isogenic mutants highlights these potential unique cellular pathways. In the *crrB151* mutant, there was activation of the a/b/c subunits of the glycerol-3-phosphate dehydrogenase enzyme,

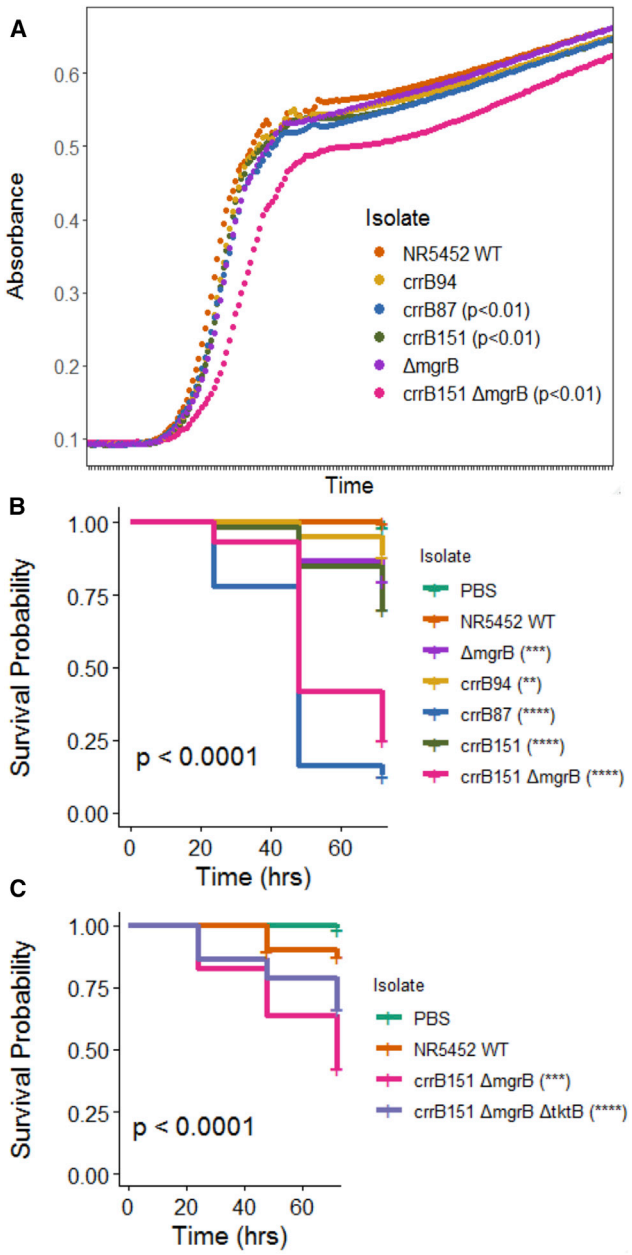

Figure 6. Growth Kinetics of Isogenic Mutants and Kaplan Curves of the Isogenic Mutants in the *G. mellonella* Killing Assays

(A) Insertion of chromosomal mutations alters the bacterial growth kinetics depending on the inserted mutation. Isolates were grown in CAMHB. Assays were completed using the EPOCH2 automated machine. Each isolate ran in triplicate, and assays were repeated at least twice. The p values were calculated via growthcurver in R.

(B) *G. mellonella* killing assays. Each isolate is injected into at least 60 larvae over three experiments. Larvae monitored for death over a 72-h span. Larval cohorts injected with *crrB94*, *ΔmgrB*, *crrB151*, *crrB151_ΔmgrB*, and *crrB87* all showed significantly increased mortality when compared to NR5452. The p values are indicated in the figure. Larvae injected with *crrB151_ΔmgrB* and *crrB87* showed significantly decreased survival when compared with all other cohorts.

(C) Larval cohorts injected with NR5452, *crrB151_ΔmgrB*, and *crrB151_ΔmgrB_ΔtktB*. The *crrB151_ΔmgrB* group was significantly more virulent when compared to the *crrB151_ΔmgrB_ΔtktB* group (p value 0.0046). Significant differences in survival analysis calculated via a log-rank test with a Bonneferoni correction (**p = 0.01, ***p = 0.001, ****p = 0.0001).

important in glycerol and lipid metabolism. In the *crrB151_ΔmgrB* mutant, there was activation of several components of the PPP, which is necessary for the production of both nicotinamide adenine dinucleotide phosphate (NADPH) and distinct carbon intermediates used for amino acid and fatty acid metabolism. The role of these pathways in virulence of Gram-negative organisms is not completely clear, but work has shown that the PPP is activated during infection. For example, in *Salmonella enterica*, the KO of the transketolase enzymes within the PPP renders the resulting mutant avirulent in a mouse model (Shaw et al., 2018; Spaans et al., 2015). One potential explanation for this could be that the upregulation of these pathways shunts carbon intermediates toward LPS biosynthesis, a key virulence factor in Gram-negative bacteria (Stincone et al., 2015).

We functionally validated a component of the RNA-seq findings via KO of the transketolase B enzyme in *crrB151_ΔmgrB*. Here, we observed a restoration of glycolytic activity and a significant decrease in virulence for the *crrB151_ΔmgrB_ΔtktB* mutant. This suggests that the PPP plays a role in virulence in *K. pneumoniae*, potentially by altering utilization of distinct carbon sources. It should be highlighted that the PPP was not activated in either of the *crrB151* or *ΔmgrB* single mutants. This suggests that the activation of multiple two-component systems (*phoP/phoQ* and *crrA/crrB*) in the PR cascade acts synergistically to alter the expression of unique cellular processes. In specific instances, this synergy increases not only polymyxin MIC, but also virulence. It will be important to further validate the RNA-seq findings to confirm the role of the other pathways described.

While our data elucidate the synergistic role of multiple mutations in the PR cascade, the explanation for why this occurs so frequently in clinical PR isolates is less clear. The answer may lie within the structural similarity between the polymyxins and antimicrobial peptides (AMPs), which are produced as an innate immune response to bacterial infections (Dobias et al., 2017). Specific AMPs, including the mammalian defensins, have a similar anti-microbial mechanism of action (Guaní-Guerra et al., 2010). Ongoing pressure from these AMPs along with intermittent polymyxin B exposure could select for isolates with multiple mutations and thus multiple mechanisms of PR. Without selection pressure, these mutations may render the isolate less fit, while the continued exposure to AMPs and the polymyxins could select for isolates with the highest MIC and virulence. This raises important antibiotic stewardship and treatment concerns for MDR *K. pneumoniae*. Unnecessary use of the polymyxins—including non-systemic administration like the inhaled, oral, or topical formulations—should be limited, as this could contribute to the selection of highly resistant and virulent isolates.

In conclusion, our data demonstrate that *crrB* missense mutations are an important cause of high-level PR in clinical CRKP isolates. While *crrB* and *mgrB* mutants share similar patterns in ArnT-mediated lipid A modifications, *crrB* mutants activate additional cellular pathways, including pEtN modification of lipid A, to confer PR. These may further account for the observed

differences in growth kinetics and virulence between different *crrB* and *crrB*151_*mgrB* double mutants. Our findings suggest that increases in MIC are advantageous in the setting of polymyxin pressure but costly in its absence. This raises concerns that the inappropriate use of polymyxins could increase the prevalence of highly resistant and virulent isolates. Our adapted single-vector CRISPR-Cas9 gene editing system provides an important tool to systematically characterize the contribution of diverse mutations to PR, virulence, and fitness in CRKP isolates. A better understanding of the complex nature of PR will aid in preventing further spread and more rationally designing diagnostic and treatment approaches.

STAR★METHODS

Detailed methods are provided in the online version of this paper and include the following:

- KEY RESOURCES TABLE
- RESOURCE AVAILABILITY
  - Lead Contact
  - Materials Availability
  - Data and Code Availability
- EXPERIMENTAL MODEL AND SUBJECT DETAILS
  - Galleria mellonella
- METHOD DETAILS
  - CRISPR-Cas9 gene editing in MDR K. pneumoniae
  - Polymyxin B susceptibility testing
  - Gene expression in WT and isogenic mutants
  - Population analysis profiles (PAPs)
  - Lipid A modifications in isogenic mutants
  - G. mellonella killing assay
  - Growth kinetics
  - Live-cell Metabolic Assays
- QUANTIFICATION AND STATISTICAL ANALYSIS
  - qRT-PCR
  - RNA-seq
  - Galleria mellonella killing assay
  - Growth Kinetics
  - Live-cell Metabolic Assays

SUPPLEMENTAL INFORMATION

Supplemental Information can be found online at https://doi.org/10.1016/j.celrep.2020.108313.

ACKNOWLEDGMENTS

This work was funded through NIH/NIAID T32 AI100852-04 and K08 AI146284 (to T.H.M.); NIH/NIAID R01 AI116939 and NIH/NIDDK U54 DK104309 (to A.-C.U.); and NIH/NIAID R01 AI150098, R01 AI129940, and R01 AI138576 (to M.S.T.).

AUTHOR CONTRIBUTIONS

This study was designed by A.-C.U. and T.H.M., with input from N.M. T.H.M. performed all genetic manipulation experiments and susceptibility testing. T.H.M. and M.K.A. performed virulence assays. M.J.G., F.D.R., M.K.A., and T.H.M. prepared sequencing libraries. C.M.H. and M.S.T. performed and interpreted all lipid A assays. F.M. aided in structural protein analyses. D.A. and G.L.B. performed metabolic assays. M.K.A. analyzed sequencing data. T.H.M. wrote the initial manuscript draft, with all authors contributing to revisions and editing. All authors approved the final manuscript.

DECLARATIONS OF INTERESTS

All authors declare no competing interests.

Received: June 9, 2020
Revised: September 16, 2020
Accepted: October 5, 2020
Published: October 27, 2020

REFERENCES

Anders, S., Pyl, P.T., and Huber, W. (2015). HTSeq–a Python framework to work with high-throughput sequencing data. Bioinformatics *31*, 166–169.

Andersson, D.I., Nicoloff, H., and Hjort, K. (2019). Mechanisms and clinical relevance of bacterial heteroresistance. Nat. Rev. Microbiol. *17*, 479–496.

Cannatelli, A., Santos-Lopez, A., Giani, T., Gonzalez-Zorn, B., and Rossolini, G.M. (2015). Polymyxin resistance caused by mgrB inactivation is not associated with significant biological cost in Klebsiella pneumoniae. Antimicrob. Agents Chemother. *59*, 2898–2900.

Cheng, Y.H., Lin, T.L., Lin, Y.T., and Wang, J.T. (2016). Amino Acid Substitutions of CrrB Responsible for Resistance to Colistin through CrrC in Klebsiella pneumoniae. Antimicrob. Agents Chemother. *60*, 3709–3716.

Cheng, Y.H., Lin, T.L., Lin, Y.T., and Wang, J.T. (2018). A putative RND-type efflux pump, H239_3064, contributes to colistin resistance through CrrB in Klebsiella pneumoniae. J. Antimicrob. Chemother. *73*, 1509–1516.

CLSI (2017). M100 Performance Standards for Antimicrobial Susceptibility Testing, 27th (Clinical and Laboratory Standards Institute).

Creecy, J.P., and Conway, T. (2015). Quantitative bacterial transcriptomics with RNA-seq. Curr. Opin. Microbiol. *23*, 133–140.

Dobias, J., Poirel, L., and Nordmann, P. (2017). Cross-resistance to human cationic antimicrobial peptides and to polymyxins mediated by the plasmid-encoded MCR-1? Clin. Microbiol. Infect. *23*, 676.e1–676.e5.

Dorman, M.J., Feltwell, T., Goulding, D.A., Parkhill, J., and Short, F.L. (2018). The Capsule Regulatory Network of *Klebsiella pneumoniae* Defined by density-TraDISort. MBio *9*, e01863.

Esposito, E.P., Cervoni, M., Bernardo, M., Crivaro, V., Cuccurullo, S., Imperi, F., and Zarrilli, R. (2018). Molecular Epidemiology and Virulence Profiles of Colistin-Resistant *Klebsiella pneumoniae* Blood Isolates From the Hospital Agency "Ospedale dei Colli," Naples, Italy. Front. Microbiol. *9*, 1463.

Giddins, M.J., Macesic, N., Annavajhala, M.K., Stump, S., Khan, S., McConville, T.H., Mehta, M., Gomez-Simmonds, A., and Uhlemann, A.C. (2018). Successive Emergence of Ceftazidime-Avibactam Resistance through Distinct Genomic Adaptations in bla_{KPC-2}-Harboring Klebsiella pneumoniae Sequence Type 307 Isolates. Antimicrob. Agents Chemother. *62*, e02101-17.

Giner, G., and Smyth, G.K. (2016). statmod: Probability Calculations for the Inverse Gaussian Distribution. R J. *8*, 339–351.

Granata, G., and Petrosillo, N. (2017). Resistance to Colistin in *Klebsiella Pneumoniae*: A 4.0 Strain? Infect. Dis. Rep. *9*, 7104.

Guaní-Guerra, E., Santos-Mendoza, T., Lugo-Reyes, S.O., and Terán, L.M. (2010). Antimicrobial peptides: general overview and clinical implications in human health and disease. Clin. Immunol. *135*, 1–11.

Haas, B.J., Chin, M., Nusbaum, C., Birren, B.W., and Livny, J. (2012). How deep is deep enough for RNA-Seq profiling of bacterial transcriptomes? BMC Genomics *13*, 734.

Hafer, C., Lin, Y., Kornblum, J., Lowy, F.D., and Uhlemann, A.C. (2012). Contribution of selected gene mutations to resistance in clinical isolates of vancomycin-intermediate Staphylococcus aureus. Antimicrob. Agents Chemother. *56*, 5845–5851.

Hankins, J.V., Madsen, J.A., Needham, B.D., Brodbelt, J.S., and Trent, M.S. (2013). The outer membrane of Gram-negative bacteria: lipid A isolation and characterization. Methods Mol. Biol. *966*, 239–258.

Henderson, J.C., O'Brien, J.P., Brodbelt, J.S., and Trent, M.S. (2013). Isolation and chemical characterization of lipid A from gram-negative bacteria. J. Vis. Exp., e50623.

Herrera, C.M., Henderson, J.C., Crofts, A.A., and Trent, M.S. (2017). Novel coordination of lipopolysaccharide modifications in Vibrio cholerae promotes CAMP resistance. Mol. Microbiol. *106*, 582–596.

Insua, J.L., Llobet, E., Moranta, D., Pérez-Gutiérrez, C., Tomás, A., Garmendia, J., and Bengoechea, J.A. (2013). Modeling Klebsiella pneumoniae pathogenesis by infection of the wax moth Galleria mellonella. Infect. Immun. *81*, 3552–3565.

Jayol, A., Nordmann, P., Brink, A., and Poirel, L. (2015). Heteroresistance to colistin in Klebsiella pneumoniae associated with alterations in the PhoPQ regulatory system. Antimicrob. Agents Chemother. *59*, 2780–2784.

Jayol, A., Nordmann, P., Brink, A., Villegas, M.V., Dubois, V., and Poirel, L. (2017). High-Level Resistance to Colistin Mediated by Various Mutations in the *crrB* Gene among Carbapenemase-Producing Klebsiella pneumoniae. Antimicrob. Agents Chemother. *61*, e01423-17.

Jeannot, K., Bolard, A., and Plésiat, P. (2017). Resistance to polymyxins in Gram-negative organisms. Int. J. Antimicrob. Agents *49*, 526–535.

Jiang, W., Bikard, D., Cox, D., Zhang, F., and Marraffini, L.A. (2013). RNA-guided editing of bacterial genomes using CRISPR-Cas systems. Nat. Biotechnol. *31*, 233–239.

Jiang, Y., Chen, B., Duan, C., Sun, B., Yang, J., and Yang, S. (2015). Multigene editing in the Escherichia coli genome via the CRISPR-Cas9 system. Appl. Environ. Microbiol. *81*, 2506–2514.

Jiang, X., Zhu, C., Lin, J., Li, J., Fu, S., and Gong, H. (2016). Vector promoters used in Klebsiella pneumoniae. Biotechnol. Appl. Biochem. *63*, 734–739.

Kidd, T.J., Mills, G., Sá-Pessoa, J., Dumigan, A., Frank, C.G., Insua, J.L., Ingram, R., Hobley, L., and Bengoechea, J.A. (2017). A *Klebsiella pneumoniae* antibiotic resistance mechanism that subdues host defences and promotes virulence. EMBO Mol. Med. *9*, 430–447.

Kwadha, C.A., Ong'amo, G.O., Ndegwa, P.N., Raina, S.K., and Fombong, A.T. (2017). The Biology and Control of the Greater Wax Moth, Galleria mellonella. Insects *8*, 61.

Langmead, B., and Salzberg, S.L. (2012). Fast gapped-read alignment with Bowtie 2. Nat. Methods *9*, 357–359.

Leung, L.M., Cooper, V.S., Rasko, D.A., Guo, Q., Pacey, M.P., McElheny, C.L., Mettus, R.T., Yoon, S.H., Goodlett, D.R., Ernst, R.K., and Doi, Y. (2017). Structural modification of LPS in colistin-resistant, KPC-producing Klebsiella pneumoniae. J. Antimicrob. Chemother. *72*, 3035–3042.

Li, H., Handsaker, B., Wysoker, A., Fennell, T., Ruan, J., Homer, N., Marth, G., Abecasis, G., and Durbin, R.; 1000 Genome Project Data Processing Subgroup (2009). The Sequence Alignment/Map format and SAMtools. Bioinformatics *25*, 2078–2079.

Macesic, N., Nelson, B., Mcconville, T.H., Giddins, M.J., Green, D.A., Stump, S., Gomez-Simmonds, A., Annavajhala, M.K., and Uhlemann, A.C. (2020). Emergence of Polymyxin Resistance in Clinical Klebsiella pneumoniae Through Diverse Genetic Adaptations: A Genomic, Retrospective Cohort Study. Clin. Infect. Dis. *70*, 2084–2091.

Nang, S.C., Morris, F.C., McDonald, M.J., Han, M.L., Wang, J., Strugnell, R.A., Velkov, T., and Li, J. (2018). Fitness cost of mcr-1-mediated polymyxin resistance in Klebsiella pneumoniae. J. Antimicrob. Chemother. *73*, 1604–1610.

Peloquin, J.J., Kuzina, L., Lauzon, C.R., and Miller, T.A. (2000). Transformation of internal extracellular bacteria isolated from Rhagoletis completa cresson gut with enhanced green fluorescent protein. Curr. Microbiol. *40*, 367–371.

Petrou, V.I., Herrera, C.M., Schultz, K.M., Clarke, O.B., Vendome, J., Tomasek, D., Banerjee, S., Rajashankar, K.R., Belcher Dufrisne, M., Kloss, B., et al. (2016). Structures of aminoarabinose transferase ArnT suggest a molecular basis for lipid A glycosylation. Science *351*, 608–612.

Ramachandran, G. (2014). Gram-positive and gram-negative bacterial toxins in sepsis: a brief review. Virulence *5*, 213–218.

Ramos, P.I., Custódio, M.G., Quispe Saji, G.D., Cardoso, T., da Silva, G.L., Braun, G., Martins, W.M., Girardello, R., de Vasconcelos, A.T., Fernández, E., et al. (2016). The polymyxin B-induced transcriptomic response of a clinical, multidrug-resistant Klebsiella pneumoniae involves multiple regulatory elements and intracellular targets. BMC Genomics *17*, 737.

Rojas, L.J., Salim, M., Cober, E., Richter, S.S., Perez, F., Salata, R.A., Kalayjian, R.C., Watkins, R.R., Marshall, S., Rudin, S.D., et al.; Antibacterial Resistance Leadership Group (2017). Colistin Resistance in Carbapenem-Resistant Klebsiella pneumoniae: Laboratory Detection and Impact on Mortality. Clin. Infect. Dis. *64*, 711–718.

Sakoulas, G., Moellering, R.C., Jr., and Eliopoulos, G.M. (2006). Adaptation of methicillin-resistant Staphylococcus aureus in the face of vancomycin therapy. Clin. Infect. Dis. *42*, S40–S50.

Selle, K., and Barrangou, R. (2015). Harnessing CRISPR-Cas systems for bacterial genome editing. Trends Microbiol. *23*, 225–232.

Shaw, J.A., Henard, C.A., Liu, L., Dieckman, L.M., Vázquez-Torres, A., and Bourret, T.J. (2018). *Salmonella enterica* serovar Typhimurium has three transketolase enzymes contributing to the pentose phosphate pathway. J. Biol. Chem. *293*, 11271–11282.

Spaans, S.K., Weusthuis, R.A., van der Oost, J., and Kengen, S.W. (2015). NADPH-generating systems in bacteria and archaea. Front. Microbiol. *6*, 742.

Stincone, A., Prigione, A., Cramer, T., Wamelink, M.M., Campbell, K., Cheung, E., Olin-Sandoval, V., Grüning, N.M., Krüger, A., Tauqeer Alam, M., et al. (2015). The return of metabolism: biochemistry and physiology of the pentose phosphate pathway. Biol. Rev. Camb. Philos. Soc. *90*, 927–963.

Sun, L., Rasmussen, P.K., Bai, Y., Chen, X., Cai, T., Wang, J., Guo, X., Xie, Z., Ding, X., Niu, L., et al. (2020). Proteomic Changes of Klebsiella pneumoniae in Response to Colistin Treatment and *crrB* Mutation-Mediated Colistin Resistance. Antimicrob. Agents Chemother. *64*, e02200-19.

Tietgen, M., Semmler, T., Riedel-Christ, S., Kempf, V.A.J., Molinaro, A., Ewers, C., and Göttig, S. (2018). Impact of the colistin resistance gene mcr-1 on bacterial fitness. Int. J. Antimicrob. Agents *51*, 554–561.

van Duin, D., and Doi, Y. (2017). The global epidemiology of carbapenemase-producing Enterobacteriaceae. Virulence *8*, 460–469.

Wang, Y., Wang, S., Chen, W., Song, L., Zhang, Y., Shen, Z., Yu, F., Li, M., and Ji, Q. (2018). Precise and efficient genome editing in Klebsiella pneumoniae using CRISPR-Cas9 and CRISPR-assisted cytidine deaminase. Appl. Environ. Microbiol. *84*, e01834-18.

Wootton, M., Howe, R.A., Hillman, R., Walsh, T.R., Bennett, P.M., and MacGowan, A.P. (2001). A modified population analysis profile (PAP) method to detect hetero-resistance to vancomycin in Staphylococcus aureus in a UK hospital. J. Antimicrob. Chemother. *47*, 399–403.

Wright, M.S., Suzuki, Y., Jones, M.B., Marshall, S.H., Rudin, S.D., van Duin, D., Kaye, K., Jacobs, M.R., Bonomo, R.A., and Adams, M.D. (2015). Genomic and transcriptomic analyses of colistin-resistant clinical isolates of Klebsiella pneumoniae reveal multiple pathways of resistance. Antimicrob. Agents Chemother. *59*, 536–543.

Yang, Q., Li, M., Spiller, O.B., Andrey, D.O., Hinchliffe, P., Li, H., MacLean, C., Niumsup, P., Powell, L., Pritchard, M., et al. (2017). Balancing mcr-1 expression and bacterial survival is a delicate equilibrium between essential cellular defence mechanisms. Nat. Commun. *8*, 2054.

Zhao, D., Yuan, S., Xiong, B., Sun, H., Ye, L., Li, J., Zhang, X., and Bi, C. (2016). Development of a fast and easy method for Escherichia coli genome editing with CRISPR/Cas9. Microb. Cell Fact. *15*, 205.

STAR★METHODS

KEY RESOURCES TABLE

REAGENT or RESOURCE	SOURCE	IDENTIFIER
Bacterial and Virus Strains		
Klebsiella pneumoniae – NR5452	Columbia University Medical Center Clinical Microbiology Laboratory	N5452
Klebsiella pneumoniae – NR5083	Columbia University Medical Center Clinical Microbiology Laboratory	NR5083
Klebsiella pneumoniae – NR4448	Columbia University Medical Center Clinical Microbiology Laboratory	NR4448
Klebsiella pneumoniae – KP0231	Columbia University Medical Center Clinical Microbiology Laboratory	KP0231
Chemicals, Peptides, and Recombinant Proteins		
Zeocin Selection Antibiotic	Invivogen	Cat# Ant-zn-5b
Polymyxin B Sulfate Salt	Sigma	Cat# 1405-20-5
Critical Commercial Assays		
Truseq mRNA stranded library preparation kit	Illumina	Cat# 20020594
Ribo-Zero rRNA depletion kit	Illumina	Cat# 20040526
Sybr Green Master Mix	Bio-rad	Cat# 1725120
RNeasy Mini Kit	QIAGEN	Cat# 74104
Restriction enzymes for CRISPR plasmid cloning	New England Biolabs	Cat# Various
Deposited Data		
RNA-seq data	This paper	Short Read Archive (NCBI) Accession# PRJNA664799 https://www.ncbi.nlm.nih.gov/bioproject/PRJNA664799
pUC19_CRISPR_*ΔpmrA*	This paper	Addgene – Catalog# 160903 https://www.addgene.org/160903/
Experimental Models: Organisms/Strains		
Galleria mellonella – NCBI:txid7137	Vanderhost Inc – Waxworms.net	Cat# "Live Wax Worms"
Oligonucleotides		
Please see Table S3	This study, Jayol et al., 2015	N/A
Software and Algorithms		
R package growthcurver – for growth kinetics analysis	RStudio	https://www.rdocumentation.org/packages/growthcurver/versions/0.3.0
R package Statmod – for growth kinetics analysis	RStudio, Giner and Smyth, 2016	https://www.rdocumentation.org/packages/statmod/versions/1.4.34
R package survminer for *Galleria* killing assay analysis	RStudio	https://cran.r-project.org/web/packages/survminer/index.html
R package survival – for *Galleria* killing assay analysis	RStudio	https://cran.r-project.org/web/packages/survival/index.html
R package DEseq2 – for RNA-seq analysis	RStudio	https://www.rdocumentation.org/packages/DESeq2/versions/1.12.3
Bowtie2	Langmead and Salzberg, 2012	http://bowtie-bio.sourceforge.net/bowtie2/index.shtml
samtools	Li et al., 2009	http://www.htslib.org
htseq	Anders et al., 2015	https://htseq.readthedocs.io/en/master/

(*Continued on next page*)

Continued

REAGENT or RESOURCE	SOURCE	IDENTIFIER
Other		
EPOCH2 Spectrophotometer	BioTek	Cat# EPOCH2
Seahorse XFe24 analyzer – for live-cell metabolic assays	Agilent	Cat# Seahorse XFe24 analyzer

RESOURCE AVAILABILITY

Lead Contact

Further information regarding this work and requests for specific reagents or more detailed protocols should be directed to Dr. Anne-Catrin Uhlemann (Au2110@columbia.edu), the lead contact who will fulfill all requests.

Materials Availability

A standard CRISPR plasmid (pUC19_CRISPR_*ΔpmrA*) is available at addgene; catalog #160903. https://www.addgene.org/160903/

Data and Code Availability

The RNA-seq datasets generated during this study is available in the NCBI Short Read Archive (SRA); accession# PRJNA664799. https://www.ncbi.nlm.nih.gov/bioproject/PRJNA664799

EXPERIMENTAL MODEL AND SUBJECT DETAILS

Galleria mellonella

NCBI:txid7137. The larvae utilized in the killing assay are ordered from Vanderhost Inc. and are shipped in a plastic container with woodchips. After receipt the larvare are stored between 60-70°C within an enclosed drawer. Larvae are used within one week of receipt, are approximately 2-4 weeks old at the time of injection, weigh approximately 250-350 mg. At the larval stage differentiation by sex is not possible given a lack of notable external sex characteristics (Kwadha et al., 2017). The *Galleria mellonella* larvae have not undergone any previous procedures, received any medications or therapy prior to use in the killing assay. No rearing of the *Galleria mellonella* or husbandry is performed. Strain, backcrossing status, genotype, health / immune status are not applicable for *Galleria mellonella* and the killing assay.

METHOD DETAILS

CRISPR-Cas9 gene editing in MDR K. pneumoniae

We optimized a single plasmid CRISPR-Cas9 / lambda red recombineering system to allow for efficient genetic manipulation in clinical MDR *K. pneumoniae* (Jiang et al., 2013; Peloquin et al., 2000; Selle and Barrangou, 2015; Wang et al., 2018; Zhao et al., 2016). For each desired single AA substitution and gene deletions we generated mutation specific CRISPR plasmids (Jiang et al., 2013; Peloquin et al., 2000; Selle and Barrangou, 2015; Wang et al., 2018; Zhao et al., 2016). We utilized a pUC19 origin of replication for gene knockouts and a PBBR1_MCS2 origin of replication for amino acid (AA) substitutions. Specific plasmid components, in addition to the origin of replication, include: (1) *Streptococcus cas9* controlled by an araBAD promoter to allow for timed expression, limiting toxicity of Cas9; (2) a guide RNA specific to the gene of interest controlled by a pTAC promoter for constitutive expression (Jiang et al., 2016); (3) a 500-1000 bp region of homology to the gene of interest containing the desired mutation (e.g., large-scale deletion, SNP); (4) lambda red recombineering genes to improve the efficiency of homologous recombination; and (5) a zeocin resistance cassette (Figure 2; Table S3) (Peloquin et al., 2000).

To generate each plasmid the Wild-type (WT) gene sequences were analyzed via the CRISPRdirect website to identify appropriate N20 sequences. N20 sequences were selected to have a melting temperature between 70-75°C and have a GC content between 40%–60%. The N20 sequences were incorporated into forward and reverse primers to amplify a gRNA cassette, controlled by the pTAC promoter, from a previously completed CRISPR plasmid as a template (Jiang et al., 2016). The desired mutation was then incorporated into gene-specific homologies. To generate missense mutations the gene specific homology was engineered to contain the desired SNP along with a series of silent mutations between the SNP and the Cas9 cut site (Figure 2). We also mutated the PAM site within the gene specific homology to ensure that following the homologous recombination event the edited bacterial chromosome would not be cut by the Cas9 protein and gRNA. The silent mutations helped increase the efficiency of homologous recombination. For gene KOs (*crrA, crrB, mgrB* and *pmrA*) the homologies were engineered to contain a 120-150bp deletion surrounding the cas9 cut site (Zhao et al., 2016; Jiang et al., 2013, 2015). Once the homologous recombination occurs the edited bacterial genome no-longer contains the N20 sequence so will not undergo further editing by the Cas9 protein and gRNA.

Sequence confirmed plasmids were inserted into the isolate to undergo genome editing. The isolate underwent serial 10% glycerol washes to make electrocompetent and stocks were stored at −80°C. Electrocompetent stocks were electroporated with the desired plasmid and reactions were plated on low salt Luria-Bertani Broth (LB) + zeocin at 1000 μg/ml. Resulting colonies were screened for the presence of the CRISPR plasmid via colony PCR with primers targeting the zeocin resistance cassette. Appropriate transformants were grown at 30°C under zeocin selection and induced with 2% arabinose after 2 hours. Following 6+ hours of induction the cultures are diluted 1:100 and plated on low salt LB + zeocin and arabinose (Zhao et al., 2016; Jiang et al., 2013, 2015). Appropriate mutants were identified with colony PCR. For gene knockouts primers bound outside of the area of homology and mutants were selected by presence of a decreased band size. For SNP insertion mutants the forward primer was designed to bind in the area of silent mutations and the reverse primer bound outside of the plasmid homology. Therefore, only the desired SNP mutant would yield a band. Mutants were further verified by Sanger sequencing (Genewiz). Mutants were cured of the CRISPR plasmid with serial passage on non-selective media. Double mutants were created by inserting the second CRISPR plasmid into an electrocompetent stock of the single mutant and repeating the knockout protocol. We performed Illumina whole genome sequencing (WGS) as previously described to ensure that no off-target editing occurred (Giddins et al., 2018).

Polymyxin B susceptibility testing

Minimum inhibitory concentrations (MICs) were determined using broth microdilution (BMD) according to CLSI guidelines (CLSI, 2017). Briefly, bacterial isolates were grown to 0.5 McFarland, diluted 1:100 in Cation-Adjusted Mueller-Hinton broth (CAMHB), and inoculated into a 96 well plate containing increasing concentrations of polymyxin diluted in CAMHB and incubated for 20-24 hours at 37°C. The positively charged polymyxins are inhibited by specific cations; the use of CAMHB therefore yields more accurate BMD results. MIC determination corresponded to the well where the bacterial button was at least less than half the size of the previous well. *In vitro* polymyxin resistance was defined as an MIC > 2 mg/L.

Gene expression in WT and isogenic mutants

Isolates were grown to mid / late log phase (OD_{600} 0.8 – 1.0) in non-selective LB broth, pelleted and whole RNA was extracted using the RNeasy kit with an imbedded on-column DNase treatment (QIAGEN). For qRT-PCR, cDNA synthesis was performed with 400ng of whole RNA utilizing the superscript II Reverse Transcription kit (Invitrogen). cDNA was used as a template for qPCR using SYBR green where each target for each isolate was run in triplicate at least four-times. *RpsL*, the small ribosomal protein gene, was used as a housekeeping gene and NR5452 (ST258) was defined as wild-type expression (Macesic et al., 2020). For RNA-Seq, whole RNA was depleted of rRNA with the RiboZero kit (Illumina). Library prep of enriched mRNA was performed with the Truseq mRNA stranded kit (Illumina), followed by sequencing using the 150 cycle v2 kit on an Illumina Miseq. Quality-filtered reads (*trimmomatic*) from all isolates were mapped against the NR5452 single contig reference genome using *bowtie2*, and *samtools* and *htseq* were used to generate read count tables (Li et al., 2009; Langmead and Salzberg, 2012; Anders et al., 2015). *DESeq2* in R was used to identify the significantly up and/or downregulated mRNA transcripts using Benjamini-Hochberg p value adjustment to obtain FDR values (Creecy and Conway, 2015; Haas et al., 2012; Ramos et al., 2016; Wright et al., 2015).

Population analysis profiles (PAPs)

PAPs on a selection of isogenic mutants were carried out as described previously (Wootton et al., 2001; Sakoulas et al., 2006; Hafer et al., 2012). In brief, single colonies were inoculated into CAMH broth and grown overnight at 37°C. Cultures were standardized to an OD_{600} of 0.5 in phosphate buffered saline. Dilutions ranging from 10^{-1} to 10^{-6} were plated with sterile beads onto CAMH Agar with the following concentrations of polymyxin B (Sigma): 0, 0.125, 0.25, 0.5, 1.0, 2.0, 4.0, 8.0, 16.0, 32.0 and 64.0 μg/ml. Colonies were counted after the plates were incubated at 37°C for 48 hours. The $\log_{10}$ CFU/ml was plotted against polymyxin B concentration using GraphPad Prism software. Experiments were repeated in duplicate.

Lipid A modifications in isogenic mutants

We analyzed lipid A profiles in the generated mutants with both thin layer chromatography (TLC) and matrix-assisted laser desorption/ionization time-of-flight mass spectrometry (MALDI-TOF). For TLC analysis, mutants were grown in LB containing ^{32}P and the lipid A purified utilizing the Caroff and Raetz approach of Bligh-Dyer extractions and mild acid hydrolysis (Henderson et al., 2013; Hankins et al., 2013). Additional lipid extractions were performed on selected mutants to verify lipid A species using MALDI-TOF mass spectrometry (Hankins et al., 2013; Henderson et al., 2013)·

G. mellonella killing assay

WT NR5452 and isogenic mutants were grown in LB broth to mid / late log phase (OD_{600} of 1.0). Each culture was pelleted and resuspended in an equal volume of PBS and adjusted to a final OD of 1.0, corresponding approximately to 5×10^8 CFUs/ml. Resuspensions were diluted 1:5 to yield a working bacterial concentration of 1×10^8 CFUs/ml. 10 μL of this resuspension was injected into the pro-leg of 20 *G. mellonella* larvae per isolate (Vanderhost incorporated) (Insua et al., 2013; Kidd et al., 2017). Serial dilutions of each isolate were plated to calculate colony-forming units (CFUs) injected to ensure comparable inoculums between isolates. We monitored for larval mortality at 24, 48 and 72 hours by tactile stimulus (Insua et al., 2013). For each experiment we injected 20 larvae with PBS as a control. We repeated each assay in triplicate for a final cohort of at-least 60 larvae per isolate. Mortality rates were

visualized with Kaplan Meier survival curves using the R package 'survminer' and significance was calculated using a Bonferroni-corrected log-rank test as implemented in the R package 'survival' (Kidd et al., 2017).

Growth kinetics

0.5 McFarland suspensions were made for all isogenic mutants and WT NR5452, diluted 1:200 in CAMHB or CAMHB with increasing concentrations of polymyxin B (up to 64 μg/ml) and grown at 37°C for 22 hours in the EPOCH2 plate reader measuring OD_{600} every 6 minutes. Each isolate was run in triplicate at least twice and results were visualized via the 'growthcurver' package in R. Statistically significant differences in growth kinetics including slope and time analysis were tested for using the R package 'statmod' (Giner and Smyth, 2016).

Live-cell Metabolic Assays

A sensor cartridge was hydrated per the manufacturer's instructions overnight at 37°C. Bacterial isolates were growth to logarithmic phase (OD_{600} of 0.5) and 10^7 CFU was added to XF base medium (Agilent) supplemented with 2mM glutamine. The bacteria were allowed to equilibrate for 1 hour at 37°C without CO_2. The extracellular acidification rate was then measured using a Seahorse XFe24 analyzer (Agilent). Each measurement cycle consisted of a mixing time of 3 minutes and a data acquisition period of 3 minutes, generating 12 data points over 73 minutes. Glucose (10 mM) was added to stimulate glycolysis, oligomycin (1 μM) to suppress oxidative phosphorylation and unleash glycolytic capacity, and 2-deoxyglucose (50 mM) to inhibit glycolysis. The area under the curve was calculated in GraphPad Prism for each individual well with the baseline defined as the first reading of each individual well.

QUANTIFICATION AND STATISTICAL ANALYSIS

qRT-PCR

Details about statistical methods used for the qRT-PCR experiments can be found in the methods paragraph describing gene expression and in the legend of Figure 3. Specifically, each gene target for each isolate was tested against the WT NR5452 at least four times. The fold change for each target was calculated via the ΔΔ method and the mean was calculated for each target gene for each isolate. Standard deviation was calculated for each target for each isolate and is shown via error bars in Figure 3. Significance was calculated by t Test and indicated with a * in Figure 3. Significance was defined as a P value of 0.05 or less.

RNA-seq

Details about the statistical methods used for the RNA-seq experiments can be found in the methods paragraph describing gene expression. Specifically, *DESeq2* in R was used to identify the significantly up and/or downregulated mRNA transcripts using Benjamini-Hochberg p value adjustment to obtain FDR values (Creecy and Conway, 2015; Haas et al., 2012; Ramos et al., 2016; Wright et al., 2015).

Galleria mellonella killing assay

Details about the statistical methods used for the *G. mellonella* killing assay can be found in the methods paragraph describing the killing assay and the legend of Figure 6. Specifically, each experiment we injected 20 larvae with each isolate being tested and 20 larvae with PBS as a negative control. We repeated each assay in triplicate for a final cohort of at-least 60 larvae per isolate. Mortality rates were visualized with Kaplan Meier survival curves using the R package 'survminer' and significance was calculated using a Bonferroni-corrected log-rank test as implemented in the R package 'survival' (Kidd et al., 2017). Significance was defined as a P value of 0.05 or less.

Growth Kinetics

Details about the statistical methods used for the growth kinetic experiments can be found in the methods paragraph describing growth kinetics and the legend of Figure 6. Specifically, to calculate statistically significant differences in growth kinetics between isolates each isolate was run in triplicate at least twice. Results were visualized via the 'growthcurver' package in R. Statistically significant differences in growth kinetics including slope and time analysis were tested for using the R package 'statmod.' A significant P value was defined 0.05 or less.

Live-cell Metabolic Assays

Details about the statistical methods used for the live cell metabolic assays be found in the methods paragraph describing the live-cell metabolic assays and the legend of Figure S4. Specifically, the area under the curve was calculated in GraphPad Prism for each individual well with the baseline defined as the first reading of each individual well. Each isolate had at least 5 readings. One-way ANOVA with a post hoc Tukey's test for multiple comparisons was performed with a P value of less than 0.05 defined as significant.